Structure and Reactivity of a Bis(μ-acetato-O,O')diiron(II) Complex, $[Fe_2(O_2CCH_3)_2(TPA)_2](BPh_4)_2$. A Model for the Diferrous Core of Ribonucleotide Reductase

Stéphane Ménage, Yan Zang, Michael P. Hendrich, and Lawrence Que, Jr.*

Contribution from the Department of Chemistry, University of Minnesota, Minneapolis, Minnesota 55455. *Received February 3, 1992*

Abstract: $[Fe_2(O_2CCH_3)_2(TPA)_2](BPh_4)_2$ (**1**, TPA = tris(2-pyridylmethyl)amine) serves as a model for the diferrous core of ribonucleotide reductase. **1** crystallizes in the space group $P\bar{1}$ (a = 10.923 (8) Å, b = 12.416 (4) Å, c = 13.935 (3) Å, α = 105.03 (3)°, β = 95.38 (3)°, γ = 92.53 (3)°, Z = 1) with an inversion center located in the center of the bis(μ-acetato)diiron(II) core. The acetates coordinate to the two Fe(II) centers in a syn-anti mode, affording an Fe-Fe separation of 4.288 (2) Å, and mediate a weak antiferromagnetic interaction between the metal centers ($H = -2JS_1 \cdot S_2$, $J \sim -1$ cm^{-1}). This dimeric structure appears to partially dissociate into monomeric units in solution, as indicated by its NMR and EPR spectra. Exposure of **1** to O_2 results in an immediate reaction forming $[Fe_2O(O_2CCH_3)_2(TPA)_2](BPh_4)_2$ (**2**), a (μ-oxo)diferric TPA complex with terminal monodentate acetates, which in turn converts readily to the previously characterized $[Fe_2O(\mu\text{-}O_2CCH_3)(TPA)_2]^{3+}$ complex (**9**) in the presence of protic solvents. Complexes **1**, **2**, and **9** represent structural motifs associated with the diiron core of ribonucleotide reductase in its diferrous and diferric oxidation states. The structural changes observed in the autoxidation of **1** mimic putative changes in the diiron site that occur in the O_2-dependent formation of oxidized ribonucleotide reductase from its reduced counterpart.

Dinuclear iron centers bridged by oxo or hydroxo groups have been found in hemerythrin (Hr), the B2 protein of ribonucleotide reductase (RRB2), and methane monooxygenase (MMO).[1] These three proteins function presumably via diiron centers having related structural features to bind dioxygen reversibly, to generate a catalytically essential tyrosyl radical, and to hydroxylate alkanes, respectively. Crystallographic studies of Hr[2] and RRB2[3] show each of the diferric forms to possess an asymmetric diiron center with an oxide bridge supported by two and one carboxylates, respectively; metHr has five terminal histidines and one available coordination site for exogenous ions, while RRB2 is more oxygen-rich with three terminal carboxylates, two histidines, and two water molecules. The diferrous forms are the relevant species that interact with dioxygen. DeoxyHr retains the same coordination environment as metHr, including the triply bridged core, except for the protonation of the oxo group to a hydroxo bridge.[4] The structure of diferrous RRB2 is still undetermined, but studies of the corresponding dimanganese active site indicate the presence of a bis(μ-carboxylato)dimetal core with no single-atom bridge.[5] In this structure, E238, which is coordinated terminally to Fe2 in a monodentate mode in the diferric form, becomes the other bridging carboxylate in the dimanganese(II) site. A similar structure may be present in the diferrous form. There is no crystallographic data on MMO, but EXAFS studies suggest an oxygen-rich environment similar to that of RRB2.[6] Indeed there appears to be some sequence homology between RRB2 and MMO with respect to their diiron binding sites.[7]

In recent years, substantial progress has been made in modeling the inactive diiron(III) biological centers using a variety of multidentate ligands and considerable insight has been gained into the magnetic and electronic properties of the diferric active sites.[1a,8] More challenging has been the synthesis of diferrous complexes, which are fewer in number. $[Fe_2(\mu\text{-}OH)(\mu\text{-}O_2CCH_3\text{-}O,O')_2(Me_3TACN)_2](ClO_4)$[9,10] (**3**) reproduces the triply bridged core present in deoxyHr,[4] while $[Fe_2(\mu\text{-}O_2CH\text{-}O)(\mu\text{-}O_2CH\text{-}O,O')_2(O_2CH)(BIPhMe)_2]$[11] (**4**), with triply bridged 5- and 6-coordinate Fe(II) centers, mimics the asymmetry found in deoxyHr. $[Fe_2(\mu\text{-}O_2CC_2H_5\text{-}O,O')_2(BPMP)](BPh_4)$[12] (**5**) also has a triply bridged core but with a μ-phenoxo bridge and exhibits integer-spin EPR signals similar to those of deoxyHrN_3 and reduced MMO;[13] these EPR signals are a result of ferromagnetic coupling between the Fe(II) centers of the diferrous unit. Other diferrous complexes with similar integer-spin signals are the bis(μ-phenoxo) complexes $[Fe_2(salmp)_2]^{2-}$[14] and $[Fe_2(H_2Hbab)(N\text{-Me-Im})(DMF)_2]$.[15] Lastly, $[Fe_2(\mu\text{-}O_2CC_6H_5\text{-}O,O')(N\text{-Et-HPTB})](BF_4)_2$[16] (**6**) has two 5-coordinate Fe(II) centers bridged by alkoxide and benzoate and is capable of binding O_2 to form a μ-peroxo intermediate. In this paper we report the synthesis, properties, and reactivity of

(1) (a) Que, L., Jr.; True, A. E. *Prog. Inorg. Chem.* **1990**, *38*, 98-200. (b) Sanders-Loehr, J. In *Iron Carriers and Iron Proteins*; Loehr, T. M., Ed.; VCH: New York, 1989; pp 373-466.

(2) (a) Holmes, M. A.; Stenkamp, R. E. *J. Mol. Biol.* **1991**, *220*, 723-737. (b) Sheriff, S.; Hendrickson, W. A.; Smith, J. L. *J. Mol. Biol.* **1987**, *197*, 273-296. (c) Stenkamp, R. E.; Sieker, L. C.; Jensen, L. H. *J. Am. Chem. Soc.* **1984**, *106*, 618-622.

(3) Nordlund, P.; Sjöberg, B.-M.; Eklund, H. *Nature* **1990**, *345*, 593-598.

(4) (a) Stenkamp, R. E.; Sieker, L. C.; Jensen, L. H.; McCallum, J. D.; Sanders-Loehr, J. *Proc. Natl. Acad. Sci. U.S.A.* **1985**, *82*, 713-716. (b) Holmes, M. A.; Le Trong, I.; Twitey, S.; Sieker, L. C.; Stenkamp, R. E. *J. Mol. Biol.* **1991**, *218*, 583-593.

(5) (a) Nordlund, P.; Uhlin, U.; Hajdu, J.; Eklund, H. *J. Inorg. Biochem.* **1991**, *43*, 534. (b) Atta, M.; Nordlund, P.; Aberg, A.; Eklund, H.; Fontecave, M. *J. Biol. Chem.*, in press.

(6) (a) Ericson, A.; Hedman, B.; Hodgson, K. O.; Green, J.; Dalton, H.; Bentsen, J. G.; Beer, R. H.; Lippard, S. J. *J. Am. Chem. Soc.* **1988**, *110*, 2330-2332. (b) DeWitt, J. G.; Bentsen, J. G.; Rosenzweig, A. C.; Hedman, B.; Green, J.; Pilkington, S.; Papaefthymiou, G. C.; Dalton, H.; Hodgson, K. O.; Lippard, S. J. *J. Am. Chem. Soc.* **1991**, *113*, 9219-9235.

(7) (a) Stainthorpe, A. C.; Lees, V.; Salmond, G. P. C.; Dalton, H.; Murrell, J. C. *Gene* **1990**, *91*, 27-34. (b) Cardy, D. L. N.; Laidler, V.; Salmond, G. P. C.; Murrell, J. C. *Mol. Microbiol.* **1991**, *5*, 335-342.

(8) Kurtz, D. M., Jr. *Chem. Rev.* **1990**, *90*, 585-606.

(9) Abbreviations used: TPA, tris(2-pyridylmethyl)amine; OBz, benzoate anion; OAc, acetate anion; BIPhMe, bis(1-methylimidazol-2-yl)phenylmethoxymethane; Me_3TACN, 1,4,7-trimethyl-1,4,7-triazacyclononane; BPMP, 2,6-bis[bis((2-pyridylmethyl)amino)methyl]-4-methylphenolate; *N*-Et-HPTB, *N,N,N',N'*-tetrakis((*N*-ethyl-2-benzimidazolyl)methyl)-2-hydroxy-1,3-diaminopropane; $HB(3,5\text{-}iPr_2pz)_3$, hydrotris(3,5-diisopropyl-1-pyrazolyl)borate; L = *N*-(carboxymethyl)glycinate; ImH = imidazole.

(10) Hartman, J. R.; Rardin, R. L.; Chaudhuri, P.; Pohl, K.; Wieghardt, K.; Nuber, B.; Weiss, J.; Papaefthymiou, G. C.; Frankel, R. B.; Lippard, S. J. *J. Am. Chem. Soc.* **1987**, *109*, 7387-7392.

(11) (a) Tolman, W. B.; Liu, S.; Bentsen, J. G.; Lippard, S. J. *J. Am. Chem. Soc.* **1991**, *113*, 152-164. (b) Rardin, R. L.; Poganiuch, P.; Bino, A.; Goldberg, D. P.; Tolman, W. B.; Liu, S.; Lippard, S. J. *J. Am. Chem. Soc.* **1992**, *114*, 5240-5249.

(12) (a) Borovik, A. S.; Que, L., Jr. *J. Am. Chem. Soc.* **1988**, *110*, 2345-2347. (b) Borovik, A. S.; Hendrich, M. P.; Holman, T. R.; Münck, E.; Papaefthymiou, V.; Que, L., Jr. *J. Am. Chem. Soc.* **1990**, *112*, 6031-6038.

(13) (a) Reem, R. C.; Solomon, E. I. *J. Am. Chem. Soc.* **1987**, *109*, 1216-1226. (b) Hendrich, M. P.; Pearce, L. L.; Que, L., Jr.; Chasteen, N. D.; Day, E. P. *J. Am. Chem. Soc.* **1991**, *113*, 3039-3044. (c) Hendrich, M. P.; Münck, E.; Fox, B. G.; Lipscomb, J. D. *J. Am. Chem. Soc.* **1990**, *112*, 5861-5865.

(14) (a) Snyder, B. S.; Patterson, G. S.; Abrahamson, A. J.; Holm, R. H. *J. Am. Chem. Soc.* **1989**, *111*, 5214-5223. (b) Surerus, K. K.; Münck, E.; Snyder, B. S.; Holm, R. H. *J. Am. Chem. Soc.* **1989**, *111*, 5501-5502.

(15) Stassinopoulos, A.; Schulte, G.; Papaefthymiou, G. C.; Carradonna, J. P. *J. Am. Chem. Soc.* **1991**, *113*, 8686-8697.

(16) Ménage, S.; Brennan, B. A.; Juarez-Garcia, C.; Münck, E.; Que, L., Jr. *J. Am. Chem. Soc.* **1990**, *112*, 6423-6425.

0002-7863/92/1514-7786$03.00/0

Table I. Crystallographic Experiments and Computations for **1**[a]

formula	$C_{88}H_{82}B_2Fe_2N_4O_4$
fw	1448.98
temp, K	182
cryst syst	triclinic
space group	$P\bar{1}$ (No. 2)
a, Å	10.923 (8)
b, Å	12.416 (4)
c, Å	13.935 (3)
α, deg	105.03 (3)
β, deg	95.38 (3)
γ, deg	92.53 (3)
V, Å^3	1813 (3)
Z	1
D(calc), g cm^{-3}	1.327
cryst dim., mm	0.60 × 0.5 × 0.40
radiation	Mo Kα (λ = 0.71069 Å)
monochromator	graphite
μ, cm^{-1}	4.56
scan type	ω
2θ max, deg	56.0
indices collected	$h,\pm k,\pm l$
no. of reflns	8759, 6987 used ($I > 3.00\sigma(I)$)
no. of least sq param	477
data/param	14.65
R^b	0.047
$R_w{}^b$	0.066
GOF[b]	1.82
p^a	0.02

[a] All calculations were performed using Texsan-Texray Structure Analysis Package, Molecular Structure Corp. (1985). The intensity data were processed as described in: *CAD 4 and SDP-PLUS User's Manual*; B. A. Frenz & Assoc.: College Station, TX, 1982. The net intensity $I = [K(\mathrm{NPI})](C - 2B)$, where $K = 20.70$ (attenuator factor), NPI = ratio of fastest possible scan rate to scan rate for the measurement, C = total count, and B = total background count. The standard deviation in the net intensity is given by $[\sigma(I)]^2 = (k/\mathrm{NPI})^2[C + 4B + (pI)^2]$, where p is a factor used to downweight intense reflections. The observed structure factor amplitude F_o is given by $F_o = (I/Lp)$, where Lp = Lorentz and polarization factors. The $\sigma(I)$'s were converted to the estimated errors in the relative structure factors $\sigma(F_o)$ by $\sigma(F_o) = {}^1/_2[\sigma(I)/I]F_o$. [b] $R = \sum|F_o - F_c|/\sum F_o$; $R_w = (\sum w|F_o - F_c|^2/\sum w(F_o)^{21/2}$; GOF = $[\sum w|F_o - F_c|^2/(N_{\mathrm{data}} - N_{\mathrm{params}})]^{1/2}$.

$[Fe_2(\mu\text{-}O_2CCH_3\text{-}O,O')_2(TPA)_2](BPh_4)_2$ (**1**), which models the putative diferrous center in reduced ribonucleotide reductase.[5]

Experimental Section

Synthetic Methods. $Fe(O_2CCH_3)_2$ and $TPA{\cdot}3HClO_4$ were prepared as described earlier.[17,18] All other reagents were used without further purification. Air-sensitive compounds were handled under argon using Schlenk techniques or in a Vacuum Atmospheres glovebox. Elemental analyses were performed at MHW Laboratories (Phoenix, AZ).

$[Fe_2(O_2CCH_3)_2(TPA)_2](BPh_4)_2$ (1). A dry methanolic solution of $TPA{\cdot}3HClO_4$ (0.296 g, 0.5 mmol) and 3.5 equiv of triethylamine (0.24 mL) was added to 1 equiv of freshly prepared $Fe(O_2CCH_3)$ (0.087 g, 0.5 mmol). The resulting bright yellow solution was stirred for 15 min until the metal salt dissolved. Metathesis by $NaBPh_4$ (0.171 g, 0.5 mmol) afforded a yellow powder (yield = 45%) which was recrystallized under an inert atmosphere by slow diffusion of diethyl ether into an acetonitrile solution. Anal. Calcd for $C_{88}H_{82}B_2Fe_2N_8O_4$ (M_r = 1448.34): C, 73.00; H, 5.70; N, 7.74. Found: C, 73.28; H, 6.15; N, 7.66. IR (KBr pellet): ν_{as}(COO) 1602 cm^{-1}.

$[Fe_2O(O_2CCH_3)_2(TPA)_2](BPh_4)_2$ (2). A 5 mM acetonitrile solution of $[Fe_2(O_2CCH_3)_2(TPA)_2](BPh_4)_2$ was exposed to air at room temperature, resulting in an immediate color change from yellow to red-brown. Slow solvent evaporation led to the formation of a polycrystalline powder. An oily product was sometimes obtained; redissolution of this oil in acetonitrile and subsequent addition of ethyl acetate afforded a brown precipitate. Anal. Calcd for $C_{88}H_{82}B_2Fe_2N_8O_5$ (M_r = 1464.34): C, 72.18; H, 5.60; N, 7.65. Found: C, 71.94; H, 5.83; N, 7.65. IR (KBr pellet): ν_{as}(COO) 1632 cm^{-1}.

Crystallographic Studies. Crystals of **1** suitable for X-ray diffraction studies were grown under Ar by diethyl ether diffusion into a dilute acetonitrile solution of the powder. A yellow prismatic crystal was mounted on a glass fiber and coated with a viscous hydrocarbon in the glovebox to prevent oxidation and possible solvent loss. Data were collected at the Crystallography Facility of the University of Minnesota Chemistry Department on an Enraf-Nonius CAD-4 diffractometer. All data were corrected for Lorentz and polarization effects. A correction for the secondary extinction coefficient was applied (coefficient = 0.939 × 10^{-6}). No decay in intensity was observed during the acquisition time. Some pertinent crystallographic details are collected in Table I, while relevant bond distances and angles are collected in Table II. Further details including the fractional atomic coordinates, thermal factors, and the complete listing of bond lengths and angles, are provided in the supplementary material. The structure was solved by direct methods.[19] The non-hydrogen atoms were refined anisotropically. Hydrogen atoms were included in the structure factor calculation in idealized positions (d_{C-H} = 0.95 Å) and were assigned isotropic thermal parameters which were 20% greater than the B_{eq} value of the atom to which they were bonded. Refinement was carried out using full-matrix least squares on F with scattering factors from ref 20 and included anomalous dispersion terms.[21]

Table II. Selected Bond Lengths (Å) and Angles (deg) for $[Fe_2(TPA)_2(OAc)_2](BPh_4)_2$ (**1**)[a]

	a. Bond Lengths		
Fe–O1C	1.998 (2)	Fe–O2C	2.145 (2)
Fe–N1	2.268 (2)	Fe–N2	2.137 (2)
Fe–N3	2.255 (2)	Fe–N4	2.146 (2)
O1C–C1C	1.267 (3)	O2C–C1C	1.242 (3)
C1C–C2C	1.511 (4)	Fe–Fe	4.288 (2)
Fe'–O2C	3.552 (2)		
	b. Bond Angles		
O1C–Fe–O2C	109.91 (7)	O1C–Fe–N1	160.85 (7)
O1C–Fe–N2	97.86 (8)	O1C–Fe–N3	87.14 (8)
O1C–Fe–N4	109.94 (9)	O2C–Fe–N1	87.56 (7)
O2C–Fe–N2	82.33 (8)	O2C–Fe–N3	162.44 (7)
O2C–Fe–N4	86.74 (8)	N1–Fe–N2	76.15 (8)
N1–Fe–N3	76.23 (8)	N1–Fe–N4	77.88 (8)
N2–Fe–N3	99.98 (8)	N2–Fe–N4	152.16 (8)
N3–Fe–N4	83.31 (8)	C1C–O1C–Fe	136.8 (2)
C1C'–O2C–Fe	138.5 (2)	O1C–C1C–O2C	125.4 (2)

[a] Estimated standard deviations in the least significant digits are given in parentheses.

Physical Methods. Visible spectra were recorded on a Hewlett Packard 8541A diode array spectrophotometer. ^{1}H NMR spectra were recorded on an IBM AC 300 or a Varian Unity 300 spectrometer at ambient temperature. Chemical shifts (in ppm) were referenced to the residual protic solvent peaks. Magnetic susceptibility data were recorded over the temperature range 2–300 K at 1 T with a SQUID susceptometer (Quantum Design, San Diego, CA) interfaced with an HP Vectra computer system. Operating procedures have been reported elsewhere.[22] IR spectra were recorded on a Perkin-Elmer FTIR 1600 Series spectrometer. Mössbauer experiments were carried out in Prof. E. Münck's laboratory by Dr. Carlos Juarez-Garcia. EPR spectra were obtained at liquid helium temperatures on a Varian E-109 spectrometer equipped with an Oxford cryostat and a cavity for parallel B_1 mode experiments.

In the manometry experiments, the quantity of dioxygen consumed in the conversion of **1** to **2** was measured with a locally constructed apparatus consisting of a mercury U-tube opened at one end to the atmosphere and connected at the other end to a temperature-controlled reaction flask which contained the solvent and the powder of **1**. The solvent was degassed by successive freeze–pump–thaw cycles and then oxygenated. After a suitable period to allow complete equilibration of the solution with its atmosphere (i.e. no change in pressure), the powder trapped above the solution was dumped into the solution and the mixture was rapidly stirred. The change in pressure was measured upon equilibration (4–6 h). The number of moles of gas taken up was calculated with the ideal gas law.

Results and Discussion

Our interest in modeling the diferrous active sites of iron–oxo proteins has led us to explore the coordination chemistry of the

(17) Hardt, H.-D.; Möller, W. *Z. Anorg. Allg. Chem.* **1961**, *313*, 57–69.
(18) Anderegg, G.; Wenk, F. *Helv. Chim. Acta* **1967**, *50*, 2330–2332.
(19) Gilmore, C. J. *J. Appl. Crystallogr.* **1984**, *17*, 42–46.
(20) Cromer, D. T.; Waber, J. T. *International Tables for X-ray Crystallography*; Kynoch Press: Birmingham, England, 1974; Vol. IV, Table 2.2 A.
(21) Cromer, D. T. *International Tables for X-ray Crystallography*; Kynoch Press: Birmingham, England, 1974; Vol. IV, Table 2.3.1.
(22) Ménage, S.; Que, L., Jr. *Inorg. Chem.* **1990**, *29*, 4293–4297.

Table III. Comparison of the Properties of Diferrous Complexes

complex	μ-OR	μ-O_2CR	r_{Fe-Fe}, Å	∠FeOFe, deg	ligand set (charge/Fe)	δ, mm/s	ΔE_Q mm/s	$-J$, cm^{-1}	ref
1, $[Fe_2(OAc)_2(TPA)_2](BPh_4)_2$		syn-anti	4.288 (2)		N_4O_2 (−1)	1.12	3.33	~1	*a*
3, $[Fe_2(OH)(OAc)_2(Me_3TACN)_2](ClO_4)$	OH	syn-syn	3.32 (1)	113.2	N_3O_3 (−1.5)	1.16	2.83	13	10
4, $[Fe_2(O_2CH)_4(BIPhMe)_2]$	O-acyl	syn-syn	3.5736 (8)	113.0	N_2O_4 (−2.5)	1.26	2.56	~0	11a
					N_2O_4 (−1.5)	1.25	3.30		
5, $[Fe_2(O_2CCH_2CH_3)_2(BPMP)](BPh_4)$	O-aryl	syn-syn	3.348 (1)	108.9	N_3O_3 (−1.5)	1.20	2.72	<0	12
$[Fe_2(salmp)_2]^{2-}$	$(O\text{-aryl})_2$			95.6					14
				95.9					
$[Fe_2(H_2Hbab)_2(N\text{-Me-Im})_2]$	$(O\text{-aryl})_2$		3.165 (7)	98.9	NO_4 (−2)	1.18	3.26	~−2.5	15
$[Fe_2(H_2Hbab)_2(N\text{-Me-Im})(DMF)_2]$	$(O\text{-aryl})_2$		3.190 (4)	97.7	NO_4 (−2)	1.27	3.35		15
				100.7	O_6 (−2)	1.30	3.00		
6, $[Fe_2(OBz)(N\text{-Et-HPTB})](BF_4)_2$	O-alkyl	syn-syn	3.473 (4)	124.0	N_3O_2 (−1)	1.07	3.13	~11	16
7, $[Fe_3(OAc)_6(BIPhMe)_2]$	O-acyl	syn-syn	3.325 (1)	105.4	O_6 (−3)	1.36	2.64	<0	11b
					N_2O_3 (−1.5)	1.14	3.60		
8, $[Fe(imidazoleacetate)_2]_n$		anti-anti	6.265 (3)		N_2O_4 (−2)	1.26	3.46	>0	24
deoxyHr	OH	syn-syn	3.32		$N_{2.5}O_3$ (−1.5)	1.14	2.76		4, 33
reduced RRB2	?		?			1.26	3.13		31
reduced MMO	?		?			1.30	3.14	<0	30

[a] This work.

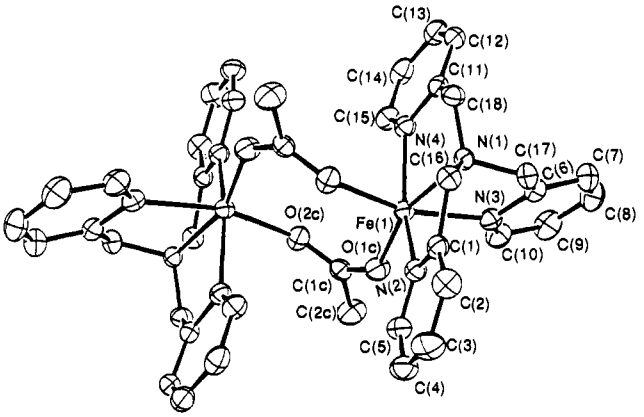

Figure 1. ORTEP plot of $[Fe_2(OAc)_2(TPA)_2]^{2+}$ (**1**) showing 50% thermal ellipsoids. Hydrogen atoms have been omitted for clarity.

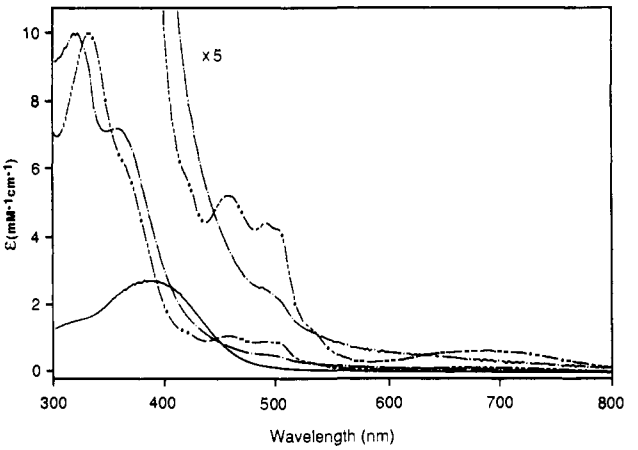

Figure 2. UV-visible spectra of **1**, **2**, and **9** in CH_3CN.

tripodal ligand TPA with $Fe(O_2CCH_3)_2$. These efforts resulted in the synthesis of $[Fe_2(\mu\text{-}O_2CCH_3\text{-}O,O')_2(TPA)_2](BPh_4)_2$ (**1**) and the characterization of its properties and reactivity toward O_2.

Crystallographic Studies of $[Fe_2(\mu\text{-}O_2CCH_3\text{-}O,O')_2(TPA)_2](BPh_4)_2$. X-ray diffraction studies show that **1** crystallizes in the triclinic space group $P\bar{1}$ with an inversion center located in the center of the bis(μ-acetato)diiron(II) core (Figure 1). Each acetate bridges the two iron atoms in an *O,O'*-mode using the syn lone pair on one carboxylate oxygen and the anti lone pair on the other. The syn-bound carboxylate oxygen exhibits the shorter bond, 1.998 (2) vs 2.145 (2) Å for the anti. The different bond lengths may arise from differences in the properties of syn and anti carboxylate lone pairs,[23] but another consideration is the fact that the syn-bound carboxylate oxygen is trans to the tertiary amine while the anti-bound carboxylate oxygen is trans to a pyridine. The syn-syn bridging carboxylates of **5** also exhibit comparable bond length differences (2.04 vs 2.14 Å), with the shorter bond trans to the tertiary amine and the longer bond trans to a pyridine.[12] Thus structural considerations may be more important than syn vs anti lone pair basicity in determining Fe–$O_{carboxylate}$ bond lengths. It is interesting to note that the Fe–O bond trans to the tertiary amine in **1** is 0.04 Å shorter than the corresponding bond in **5**. We interpret this difference as arising from the presence of the phenolate bridge in **5**, which decreases the Lewis acidity of the Fe(II) centers relative to **1** and engenders the slightly longer Fe–$O_{carboxylate}$ bond.

Table III compares the properties of the bis(μ-acetato)diiron(II) core with those of other diferrous complexes. The syn-anti bridging mode of the acetates affords a metal–metal distance of 4.288 (2) Å, longer than those found for complexes with syn-syn carboxylate bridges like **3**–**6**, having Fe–Fe distances of 3.3–3.6 Å,[10-12,16] but shorter than that of **8** with anti-anti carboxylate bridges (6.265 (3) Å).[24] For complexes **3**–**6**, the Fe–Fe distance is modulated by the nature of the single-atom bridge (i.e. hydroxo, formato-*O*, phenoxo, and alkoxo, respectively). **1** is thus far the only diiron complex to exhibit a syn-anti carboxylate bridging mode; perhaps the absence of a single-atom bridge between the metal centers removes the constraint imposed by such a bridge for a syn-syn bridging mode and allows the carboxylates to adopt the sterically less demanding syn-anti mode. Other examples of this bridging mode include $[Mn_2(bipy)_4(OAc)_2]^{2+}$,[25a] $[Mn_2(bpen)_2(OAc)_2]^{2+}$,[25b] and $[Cu_2L_2(ImH)_4]$;[26] in the last case, the carboxylate is part of the tridentate L and is constrained to bridge in the syn-anti mode. These complexes have similarly large metal–metal separations, 4.583 (1), 4.298, and 5.030 (1) Å, respectively.

The four nitrogens of TPA complete the distorted octahedral environment on each iron and adopt the characteristic configuration of such tripods with N_{amine}–Fe–N_{py} angles averaging ~77° to accommodate the five-membered chelate rings.[12,27] The Fe–N_{amine} bond is expectedly long (2.268 (2) Å) and trans to the syn carboxylate oxygen. The Fe–N_{py} bond trans to the anti carboxylate oxygen is also long (2.255 (2) Å), while the two pyridine

(23) (a) Gandour, R. B. *Bioorg. Chem.* **1981**, *10*, 169–176. (b) Allen, F. H.; Kirby, A. J. *J. Am. Chem. Soc.* **1991**, *113*, 8829–8831.

(24) Martinez-Lorente, M.-A.; Tuchagues, J.-P.; Pétroulêas, V.; Savariault, J.-M.; Poinsot, R.; Drillon, M. *Inorg. Chem.* **1991**, *30*, 3587–3589.

(25) (a) Rardin, R. L.; Tolman, W. B.; Lippard, S. J. *New J. Chem.* **1991**, *15*, 417–430. (b) Che, C.-M.; Tang, W.-T.; Wong, K.-Y.; Wong, W.-T.; Lai, T.-F. *J. Chem. Res.* **1991**, 30.

(26) Dung, N.-H.; Viossat, B.; Busnot, A.; Sicilia Zafra, A. G.; Gonzales Perez, J. M.; Niclos Guttierez, J. *Inorg. Chim. Acta* **1990**, *169*, 9–12.

(27) (a) Yan, S.; Cox, D. D.; Pearce, L. L.; Juarez-Garcia, C.; Que, L., Jr.; Zhang, J. H.; O'Connor, C. J. *Inorg. Chem.* **1989**, *28*, 2507–2509. (b) Norman, R. E.; Yan, S.; Que, L., Jr.; Backes, G.; Ling, J.; Sanders-Loehr, J.; Zhang, J. H.; O'Connor, C. J. *J. Am. Chem. Soc.* **1990**, *112*, 1554–1562.

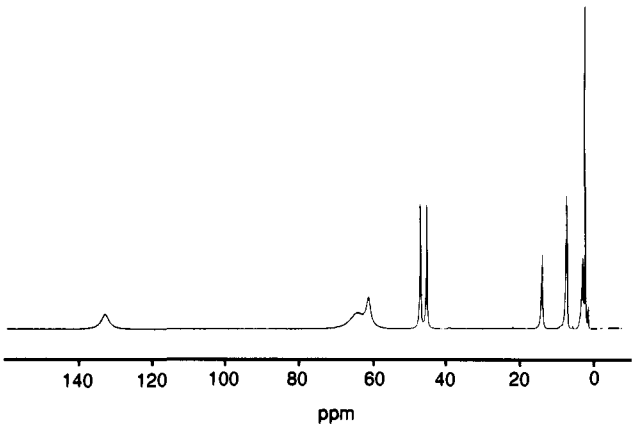

Figure 3. ^1H NMR spectrum of **1** in CD_3CN.

Table IV. NMR Shifts

assgnt	1	2	9	10
py α or CH_2	133 (0.6)	32	36	
			31	30
	64.1 (1.2)		23	29
			20	20
py β	47.0 (8.9)	16.1	17.4	17.7
	45.2 (11.1)		16.5	16.7
			12.6	
			12.3	12.9
			11.2	11.5
py γ	13.7 (26.1)	7.5	7.9	7.5
			6.9	7.1
			6.5	
OAc	61.2 (3.9)	8.7	14.2	

nitrogen atoms trans to each other have shorter Fe–N bond lengths (2.137 (2) and 2.146 (2) Å). The values observed for **1** are comparable to those found for **5**.[12]

Physical Properties of 1. Complex **1** exhibits a broad UV absorption band centered near 388 nm (ϵ 2.6 mM^{-1} cm^{-1}) (Figure 2). Its ^1H NMR spectrum in CD_3CN at 298 K (Figure 3) exhibits relatively sharp features, as expected from the short T_{1e} of a high-spin ferrous center. The number of pyridine peaks observed shows that the TPA ligand has effective 3-fold symmetry in solution and suggests that there is a facile exchange process that averages the environments of the three pendant pyridines; dissociation of the dimer into monomeric units would seem to be a likely explanation. The NMR peak assignments (Table IV) are deduced from peak integrations, deuterium substitution, and T_1 measurements. The py α protons, which are closest to the metal centers (~3.2 Å), are assigned to the 133 ppm peak due to its broadness. The β protons on each pyridine (~5 Å) are resolved from each other and assigned to features at 45.2 and 47.0 ppm. The py γ protons are found at 13.7 ppm. These assignments are consistent with those made for the pyridine protons in **5** and related complexes.[12b,28] The acetate CH_3 protons are assigned by deuterium substitution to the peak at 61.2 ppm which overlaps with the methylene ligand protons at 64.1 ppm. The large shift observed for the acetate is comparable to the acetate methyl shift (50 ppm) observed for the acetate analogue of **5**.[12b] The larger shift for **1** probably reflects its shorter $Fe–O_{carboxylate}$ bond, which enhances the delocalization of unpaired spin density from the Fe(II) center. The isotropic shift of acetate methyl protons in iron complexes is rather variable[29] and depends not only on the iron oxidation state but also on the strength of the metal–carboxylate interaction. Significantly larger shifts are observed for complexes where the metal center and the carboxylate group form a plane; such a planar arrangement would enhance π interactions between the metal and the carboxylate orbitals and result in a greater delocalization of unpaired spin density onto the methyl group.

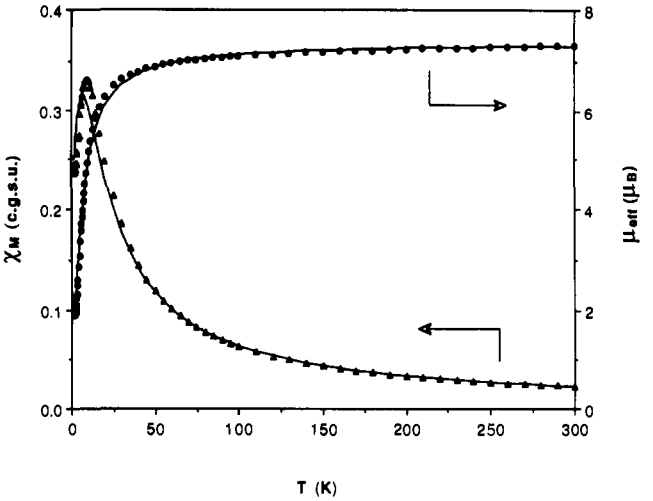

Figure 4. Temperature dependence of the magnetic susceptibility and the magnetic moment of **1** at 1 T with corresponding fits to the data.

The Mössbauer spectrum of **1** displays one quadrupole doublet (Γ = 0.26 mm/s) with δ = 1.12 mm/s and ΔE_Q = 3.33 mm/s, indicative of a rather anisotropic electronic environment. The ΔE_Q value of **1** is listed together with those of other diferrous complexes in Table III and found to be comparable to those of the diferrous forms of MMO[30] and RRB2.[31] Since the quadrupole splitting (ΔE_Q) is a measure of the electric field gradient about the metal center, earlier papers have suggested that ferrous sites with larger ΔE_Q values may correspond to 5-coordinate sites which are likely to have electronic environments that are anisotropic.[11,15] However **1** and **8**,[32] both of which have 6-coordinate sites, have ΔE_Q values that are comparable to those of 5-coordinate sites, thereby demonstrating that 6-coordinate sites under appropriate circumstances can engender distortions in the Fe(II) electronic environment similar to those imposed by 5-coordinate sites. These observations indicate that ΔE_Q values for high-spin Fe(II) complexes cannot be used reliably as an indicator of coordination number.

A perusal of Table III, however, suggests isomer shift values may be useful for probing electron density at the Fe(II) center. The data in Table III suggest that δ increases with coordination number and the number of anionic ligands bound. Nitrogen-rich sites have values that approach 1.1 mm/s, while oxygen-rich sites have values near 1.3 mm/s. Consistent with this trend, deoxyHr[33] exhibits an isomer shift similar to those of **1** and **3**. Both reduced RRB2[31] and reduced MMO[30] with respective isomer shifts of 1.26 and 1.30 mm/s would then be expected to have coordination environments more oxygen-rich than that of deoxyHr. For RRB2, the Mössbauer data indicates that the carboxylate-rich diiron site found for the diferric form by X-ray crystallography[3] is maintained in the diferrous form. The notion of a similarly oxygen-rich environment for MMO is supported by results derived from EXAFS analysis, which reveals a short average Fe–(O/N) bond distance.[6]

The magnetic properties of **1** have been investigated at 1 T over a temperature range of 2–300 K (Figure 4). At ambient temperature, its magnetic moment is 7.3 μ_B, consistent with the presence of two noninteracting high-spin ferrous centers in the molecule. Its magnetic moment drops precipitously below 40 K and the χ vs T plot exhibits a Neel temperature of 9 K, indicating a weak antiferromagnetic interaction between the two ferrous centers. Fitting the data with the Heisenberg Hamiltonian $H = -2JS_1 \cdot S_2$, where $S_1 = S_2 = 2$,[34] we found $J \sim -1$ cm^{-1}.[35]

(28) Ming, L.-J.; Jang, H. G.; Que, L., Jr. *Inorg. Chem.* **1992**, *31*, 359.
(29) Arafa, I. M.; Goff, H. M.; David, S. S.; Murch, B. P.; Que, L., Jr. *Inorg. Chem.* **1987**, *26*, 2779–2784.
(30) Fox, B. G.; Surerus, K. K.; Münck, E.; Lipscomb, J. D. *J. Biol. Chem.* **1988**, *263*, 10553–10556.
(31) Lynch, J. B.; Juarez-Garcia, C.; Münck, E.; Que, L., Jr. *J. Biol. Chem.* **1989**, *264*, 8091–8096.
(32) Rardin, R. L.; Bino, A.; Poganiuch, P.; Tolman, W. B.; Liu, S.; Lippard, S. J. *Angew. Chem., Int. Ed. Engl.* **1990**, *29*, 812–814.
(33) Clark, P. E.; Webb, J. *Biochemistry* **1981**, *20*, 4628–4632.
(34) O'Connor, C. J. *Prog. Inorg. Chem.* **1982**, *29*, 203.

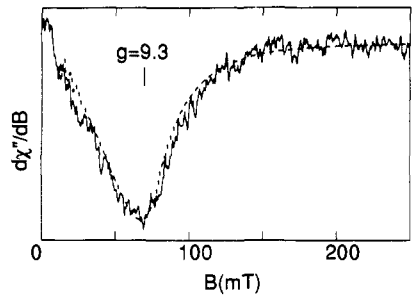

Figure 5. X-band EPR spectrum of **1** in CH_3CN (0.5 mM) obtained in parallel B_1 mode at 2.5 K (traced line). The simulation (dashed line) is for $S = 2$, $g = 2.0$, $\Delta \sim 0.4$ cm^{-1}, and $\sigma_\Delta \sim 0.2$ cm^{-1}, where Δ is the zero-field splitting of the EPR active doublet. Quantitation of the spectrum gives ~0.1 mM Fe(II). Spectral parameters: microwave power, 0.2 mW at 9.083 GHz; modulation, 1 mT at 100 kHz; gain, 4×10^4; dB/dt, 1.7 mT/s; time constant, 0.25 s.

However, because zero-field splitting (D) values for high-spin Fe(II) are comparable to or larger than 1 cm^{-1} and complicated energy level distributions arise when $|J| \leq |D|$, zero-field splitting terms cannot be neglected in this analysis. Thus a multi-field magnetization study is needed, in conjunction with fits utilizing a spin Hamiltonian that includes zero-field splitting terms, in order to obtain a more accurate picture of the magnetic properties of **1**.[36]

The magnetic data for **1** nevertheless show that bridging bidentate carboxylates can promote weak antiferromagnetic coupling interactions between two metals centers despite being separated by 4.288 (2) Å. The interactions promoted appear small but comparable to that found for **8** with its anti-anti carboxylate bridges,[24] in contrast to the larger values found for **3** ($J = -13$ cm^{-1})[10] and **6** ($J = -11$ cm^{-1}).[16] It appears that single-atom bridges such as hydroxo and alkoxo groups more effectively mediate antiferromagnetic coupling in diiron(II) complexes. However other factors must also come into play, since the magnetic properties of **4** and **5** significantly differ from those of **3** and **6**. Complex **4** with its (μ-formato-*O*)bis(μ-carboxylato-*O*,*O*')diiron(II) core exhibits very weak or no coupling, despite the fact that it possesses a single-atom bridge and has an Fe-μ-O-Fe angle almost identical to that of **3**.[11] Perhaps the significantly longer Fe-μ-O bonds in **4** (av 2.14 Å) relative to those of **3** (1.99 Å) and **6** (1.96 Å) are responsible for the much weaker interactions, by analogy to the correlation noted for diferric complexes between bridge bond length and coupling strength.[37] Complex **5** with its (μ-phenoxo)bis(μ-carboxylato-*O*,*O*')diiron(II) core has intermediate Fe-μ-O bond lengths of 2.05–2.06 Å but appears to exhibit ferromagnetic interactions from the temperature behavior of its integer-spin EPR signal.[12] In this case, it is likely that its more acute Fe-O-Fe angle (108.9°) enhances the ferromagnetic coupling interaction. Other diferrous complexes that are ferromagnetically coupled are bis(μ-phenoxo) complexes which have Fe-μ-O-Fe angles of 96–100°.[14,15]

The EPR spectrum of **1** in CH_3CN consists of a broad feature with a minimum at $g = 9.3$ (Figure 5), in stark contrast to the $g = 16$–18 signals observed for a number of diferrous complexes, which result from ferromagnetic interactions between Fe(II) centers.[12,13] The $g = 9.3$ signal is characteristic of an $S = 2$ center and indicates the presence of uncoupled high-spin Fe(II) species;[38] this signal, which is not observed in the solid state, represents (10 ± 5)% of the iron in the sample on the basis of the simulation displayed in Figure 5 and obtained by following previously discussed spin quantitation methods.[38] The appearance of the $g =$ 9.3 signal in CH_3CN solution implies that dimeric **1** may partially dissociate into monomers upon dissolution, a suggestion consistent with the NMR observations (vide supra). That the bulk of the sample is EPR silent is due not to the inaccessibility of paramagnetic states in this weakly coupled system but to zero-field splitting effects that separate levels by gaps larger than the microwave quantum at X-band.

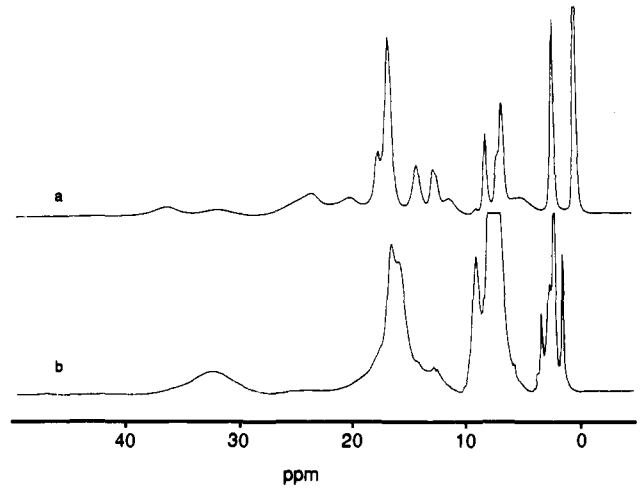

Figure 6. ^{1}H NMR spectra of (a) **9** and (b) **2** in CD_3CN.

Reactivity with O_2. The reaction of the diferrous forms of the iron–oxo proteins, such as Hr, RRB2, and MMO, with dioxygen is a key element of their respective functions. Thus the reactivity of synthetic diferrous complexes with O_2 is of great interest. Upon exposure to O_2, **3** yields the corresponding (μ-oxo)diferric complex,[10] while **5** affords the corresponding mixed valent derivative;[12] both these complexes are coordinatively saturated, and the products appear to result from autoxidation. On the other hand, both **4** and **6** have available coordination sites for O_2 binding. Thus exposure to O_2 converts **4** from a (μ-formato-*O*)bis(μ-formato-*O*,*O*')diiron(II) species to a (μ-oxo)bis(μ-formato-*O*,*O*')diiron(III) complex with the oxo group derived from O_2.[11] Complex **6** yields a metastable (−60 °C) O_2 adduct that is characterized as a (μ-1,2-peroxo)diiron(III) species.[16]

The addition of O_2 at 20 °C to the bright yellow acetonitrile solution of **1** rapidly turns the solution red-brown, from which a brown powder, **2**, can be obtained upon solvent evaporation. Complex **2** affords an elemental analysis consistent with the formulation $[Fe_2O(O_2CCH_3)_2(TPA)_2](ClO_4)_2$. Its spectroscopic properties can be compared with those of two related complexes that are crystallographically characterized, $[Fe_2O(O_2CCH_3)(TPA)_2](ClO_4)_3$ (**9**), which is an unsymmetric dinuclear complex with a (μ-oxo)(μ-carboxylato)diiron(III) core,[27] and $[Fe_2OCl_2(TPA)_2](ClO_4)_2$ (**10**), which is a centrosymmetric complex with a linear oxo bridge.[39]

Complex **2** exhibits UV–visible bands at 320 nm ($\epsilon = 10.0$ mM^{-1} cm^{-1}), 360 nm (8 mM^{-1} cm^{-1}), and 500 nm (sh) (Figure 2). These features differ from those of **9**, particularly in the 400–700-nm region where several transitions with oxo-to-Fe(III) charge-transfer character are observed in complexes with bent Fe–O–Fe units.[39] The featureless visible region of **2** is reminiscent of that of **10**, which has a linear Fe–O–Fe unit.[39]

The ^{1}H NMR spectrum of **2** in CD_3CN shows features only in the 0–40 ppm range (Table IV) and confirms that it is a $[Fe^{III}_2O(TPA)_2]$ complex like **9** and **10** (Figure 6).[27,39] The multiplicity of the TPA ligand resonances is indicative of the mode of TPA binding to the iron centers in such complexes. In **9**, one TPA binds with the amine trans to the oxo bridge, while the other TPA binds with a pyridine trans to the oxo bridge. This inequivalence gives rise to four different pyridine ring environments and is reflected by the complexity of its NMR spectrum. In **10**,

(35) We have not included a fit of the data including a term for a paramagnetic impurity on the following grounds. We can eliminate the presence of a ferric impurity by the absence of appropriate EPR signals; an impurity if present would then have to be a mononuclear ferrous species, which would be difficult to distinguish from a diferrous species with very weak antiferromagnetic coupling, as is the case with **1**.

(36) Day, E. P.; David, S. S.; Peterson, J.; Dunham, W. R.; Bonvoisin, J. J.; Sands, R. S.; Que, L., Jr. *J. Biol. Chem.* **1988**, *263*, 15561–15567.
(37) Gorun, S. M.; Lippard, S. J. *Inorg. Chem.* **1991**, *30*, 1625–1630.
(38) Hendrich, M. P.; Debrunner, P. G. *Biophys. J.* **1989**, *56*, 489–506.
(39) Norman, R. E.; Holz, R. C.; Ménage, S.; O'Connor, C. J.; Zhang, J. H.; Que, L., Jr. *Inorg. Chem.* **1990**, *29*, 4629–4637.

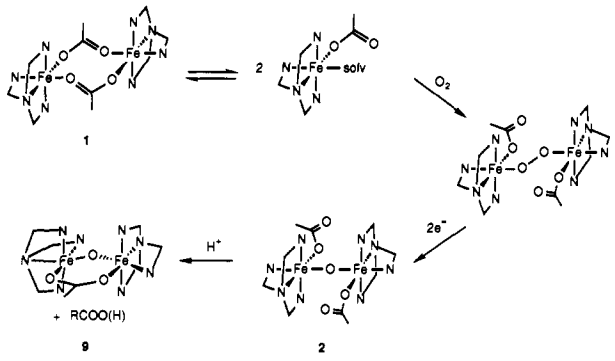

Figure 7. Proposed reaction scheme for the autoxidation of **1**.

the iron centers are equivalent with pyridines coordinated trans to the oxo bridge; correspondingly, there are only two types of pyridine rings and thus fewer NMR features. The pattern of the TPA features in the NMR spectrum of **2** is indicative of a complex analogous to **10**.

The coordination modes of the acetate ligands differ in **2** and **9**. In the IR spectra, the ν_{as}(COO) shifts from 1632 cm^{-1} for **2** to 1607 cm^{-1} for **9**, which suggests a monodentate binding mode for the acetates in **2**.[40,41] Furthermore, the acetate CH_3 resonance of **2**, assigned by deuterium substitution, is found at 8.7 ppm, in contrast to 14.0 ppm for the μ-acetato CH_3 in **9**. The smaller isotropic shift of the acetate signal in **2** (approximately half that of **9**) indicates a less efficient transmission of unpaired spin density, which we would ascribe to a monodentate acetate coordinated via its anti lone pair.[29] On the basis of these comparisons, we propose that **2** is a (μ-oxo)diferric TPA complex with monodentate terminal acetates (see Figure 7).

Depending upon the preparation, the formation of a small amount of **9** in the reaction of **1** with O_2 can be observed by NMR. The presence of **9** is indicated by a small signal at 14 ppm associated with the bridging acetate and is confirmed by ^{2}H-NMR data on the oxidation of $[Fe_2(OAc\text{-}d_3)_2(TPA)_2]^{2+}$, which show a large resonance at 8.7 ppm (terminal OAc) and a smaller feature at 14 ppm (bridging OAc). The formation of **9** is enhanced by the presence of methanol or water. Indeed **2** is readily converted to **9** when water is added. It thus seems likely that the oxidation of **1** affords **2**, which in turn yields **9** in the presence of protic solvent.

The conversion of **1** to **2** requires 0.6 (1) mole of dioxygen or approximately 4 Fe(II) atoms oxidized/O_2 consumed, a ratio also observed for the autoxidation of **4** and Fe(II) porphyrins.[42] A plausible mechanism for this conversion is shown in Figure 7. The autoxidation of **1** is probably initiated by the interaction of O_2 with monomeric units of **1**, which form in acetonitrile as suggested by the NMR and EPR data. Such monomeric units would either be coordinatively unsaturated or have a readily displaceable bound solvent molecule. Reaction of this O_2 adduct with a second monomeric unit would then afford a (μ-peroxo)diiron(III) complex, similar in structure to that proposed for the recently observed dinuclear O_2 adduct of mononuclear $[Fe\{HB(3,5\text{-}iPr_2pz)_3\}(OBz)(CH_3CN)]$.[43] The ($\mu$-peroxo)diiron(III) complex would then be reduced by its ferrous precursors to yield two (μ-oxo)diiron(III) molecules. Such an autoxidation mechanism follows closely that established for porphyrin complexes by NMR studies wherein the participation of intermediate species such as $[(Por)Fe^{II}O_2]$, $[(Por)Fe^{III}\text{–}O\text{–}O\text{–}Fe^{III}(Por)]$, and $[(Por)Fe^{IV}{=}O]$ has been established.[42] However we have not been able to detect any intermediates in the autoxidation of **1** even at −80 °C. It is likely, for example, that the absence of sterically encumbering alkyl groups on the TPA ligand, as has been designed into $[Fe\{HB(3,5\text{-}iPr_2pz)_3\}(OBz)(CH_3CN)]$,[43] hampers the stabilization of the corresponding (μ-peroxo)diiron(III) derivative and facilitates its reduction by its ferrous precursors to form the observed (μ-oxo)diiron(III) products.

Relevance to Ribonucleotide Reductase

We have determined the structure of a bis(μ-carboxylato-*O*,*O'*)diferrous complex which, upon exposure to dioxygen, affords a (μ-oxo)diferric complex with terminal carboxylates in aprotic media and a (μ-oxo)(μ-carboxylato)diferric complex in the presence of protons. This chemistry may be analogous to the structural changes associated with the diiron site in ribonucleotide reductase as it converts from the diferrous form[44] to the diferric form.[3] The relevance of a bis(μ-carboxylato)diferrous structural motif for $RRB2_{red}$ is suggested by the crystal structure for the Mn(II)-reconstituted RRB2, where the metal centers appear to be bridged by the carboxylates of E115 and E238 with no evidence for a single-atom bridge.[5] If this coordination scheme is maintained in diferrous RRB2, then **1** can serve as a structural model for such a site. However there are several differences between **1** and the putative diferrous RRB2 active site. (1) The bridging carboxylates in the protein are likely to be bound in a syn-syn mode, as found in the dimanganese derivative,[5] since the protein pocket containing the diiron site may not be able to accommodate the larger Fe–Fe separation required by syn-anti carboxylate bridges. (2) The diiron unit in $RRB2_{red}$ is oxygen-rich in ligation[3,5] and has available coordination sites,[45] while **1** is nitrogen-rich and coordinatively saturated. (3) **1** exhibits weak antiferromagnetic coupling, while diferrous RRB2 shows integer-spin EPR signals near $g = 16$ that suggest ferromagnetic coupling.[46]

Despite these structural differences, **1** serves as a reactivity model for $RRB2_{red}$. $RRB2_{red}$ reacts readily with O_2, converting the putative bis(μ-carboxylato)diferrous site into a (μ-oxo)diferric center. In the oxidized form, the E115 carboxylate remains bridged to the diiron unit, but E238 swings away from Fe1 and remains coordinated only to Fe2 in a monodentate fashion.[3] The oxidation of **1** to **2** also occurs facilely. In CH_3CN, the oxidation results in the conversion of both its carboxylate bridges into terminal carboxylates,[47] a change in carboxylate coordination mode also ascribed to E238 in the oxidation of $RRB2_{red}$. However, in the presence of protons, a (μ-oxo)(μ-carboxylato)diferric core analogous to that found in RRB2 forms. The loss of a terminal acetate in the conversion of **2** to **9** can probably be ascribed to the lack of available coordination sites and the stability of the tetradentate TPA–iron(III) interaction. In the reaction of $RRB2_{red}$ with O_2, the availability of a coordination site for E238 on Fe2 allows it to remain coordinated as a terminal ligand when the oxo bridge forms.

The stoichiometry for the oxidation of **1** is 4 Fe(II)/O_2 consumed. Similar stoichiometries are found for the autoxidation of **4**,[11] Fe(II) porphyrins,[42] and the Y122F mutant form of $RRB2_{red}$.[48] These observations imply that the putative (μ-peroxo)diferric intermediates in the oxidations of **1** and Y122F-$RRB2_{red}$ are both readily reduced by their respective diferrous precursors in the absence of other oxidizable species. Indeed Stubbe and co-workers have recently reported transient species in the oxidation of $RRB2_{red}$ with O_2 whose lifetimes are shortened when reducing equivalents are available.[49] In the case of RRB2, the catalytically essential Y122 residue can provide one electron

(40) Nakamoto, K. *Infrared and Raman Spectra of Inorganic and Coordination Compounds*, 4th ed.; Wiley: New York, 1986; pp 231–233.
(41) Deacon, G. B.; Phillips, R. J. *Coord. Chem. Rev.* **1980**, *33*, 227.
(42) Latos-Grazynski, L.; Cheng, R.-J.; La Mar, G. N.; Balch, A. L. *J. Am. Chem. Soc.* **1982**, *104*, 5992–6000.
(43) Kitajima, N.; Fukui, H.; Moro-oka, Y.; Mizutani, Y.; Kitagawa, T. *J. Am. Chem. Soc.* **1990**, *112*, 6402–6403.
(44) Sahlin, M.; Gräslund, A.; Petersson, L.; Ehrenberg, A.; Sjöberg, B.-M. *Biochemistry* **1989**, *28*, 2618–2625.
(45) McCormick, J. M.; Reem, R. C.; Forough, J.; Bollinger, J. M.; Jensen, G. M.; Stephens, P. J.; Stubbe, J.; Solomon, E. I. *New J. Chem.* **1991**, *15*, 439–444.
(46) Hendrich, M. P.; Elgren, T. E.; Que, L., Jr. Work in progress.
(47) The conversion of a formato-*O* bridge to a terminal formate in the autoxidation of **4** has been postulated to involve a "carboxylate shift" mechanism;[25a] it seems less likely that a carboxylato-*O* bridge would be involved in the autoxidation of **1**.
(48) Elgren, T. E.; Lynch, J. B.; Juarez-Garcia, C.; Münck, E.; Sjöberg, B.-M.; Que, L., Jr. *J. Biol. Chem.* **1991**, *266*, 19265–19268.
(49) Bollinger, J. M., Jr.; Edmondson, D. E.; Huynh, B. H.; Filley, J.; Norton, J. R.; Stubbe, J. *Science (Washington, D.C.)* **1991**, *253*, 292–298.

and becomes oxidized to its radical form, thereby generating the active RRB2.[49] However, in the case of **1**, we have been unable to intercept the putative peroxo intermediate with appropriate substrates.

Acknowledgment. This work was supported by funds from the National Institutes of Health (Grant GM-38767) and the University of Minnesota Graduate School. We thank Dr. Carlos Juarez-Garcia and Professor Eckard Münck for providing the Mössbauer spectrum of **1** and Dr. Ho G. Jang for his valuable assistance with the magnetic susceptibility experiments and their analysis.

Supplementary Material Available: Tables listing fractional atomic coordinates, thermal factors, and all bond lengths and angles for **1** and Figure S1, showing the Mössbauer spectrum of **1** and its theoretical fit (18 pages). Ordering information is given on any current masthead page.

The Intercalation Reaction of Pyridine with Manganese Thiophosphate, $MnPS_3$

Pattayil Alias Joy and Sukumaran Vasudevan*

Contribution from the Department of Inorganic and Physical Chemistry, Indian Institute of Science, Bangalore-560012, India. *Received March 27, 1992*

Abstract: The intercalation of pyridine in the layered manganese thiophosphate, $MnPS_3$, has been examined in detail by a variety of techniques. The reaction is interesting since none of the anticipated changes in optical and electrical properties associated with intercalation of electron donating molecules is observed. The only notable change in the properties of the host lattice is in the nature of the low-temperature magnetic ordering; while $MnPS_3$ orders antiferromagnetically below 78 K, the intercalated compound shows weak ferromagnetism probably due to a canted spin structure. Vibrational spectra clearly show that the intercalated species are pyridinium ions solvated by neutral pyridine molecules. The corresponding reduced sites of the host lattice, however, were never observed. The molecules in the solvation shell are exchangeable. Although the reaction appears to be topotactic and reversible, from XRD, a more detailed analysis of the products of deintercalation reveal that it is not so. The intercalation proceeds by an ion exchange/intercalation mechanism wherein the intercalated species are pyridinium ions solvated by neutral molecules with charge neutrality being preserved not by electron transfer but by a loss of Mn^{2+} ions from the lattice. The experimental evidence leading to this conclusion is discussed and it is shown that this model can account satisfactorily for the observed changes (or lack of it) in the optical, electrical, vibrational, and magnetic properties.

I. Introduction

The intercalation reaction in layered lattices provides a unique route to the study of host-guest interactions in various environments.[1,2] In this paper we report a detailed investigation of the intercalation in the layered transition metal thiophosphates,[3] MPS_3, using the Lewis base pyridine as a probe guest species. What makes the transition metal thiophosphates interesting is that although they bear a strong structural resemblance (Figure 1) to the well-studied transition metal dichalcogenides,[4,5] MX_2, and like them can intercalate a wide variety of electron donating molecules[6] within the van der Waals gap the nature of metal-ligand interactions is much more ionic[7] as compared to the transition metal dichalcogenides. This provides a unique opportunity to contrast the behavior and properties of the same guest molecule intercalated in structurally similar lattices possessing widely different types of bonding.

In light of numerous experimental investigations,[7,8] it is generally agreed that MPS_3 compounds are best viewed as salts of the thiophosphate anion, $M_2^{2+}(P_2S_6)^{4-}$, rather than as metal phosphorus sulfides. The M^{2+} ions are in the high spin state, and the compounds are magnetic undergoing a low-temperature magnetic transition to an antiferromagnetic state.[9] In contrast the M-X bonds in the transition metal dichalcogenides are much more covalent, and a much better description of the d electrons is the band model.[5]

The intercalation behavior of the transition metal dichalcogenides is well documented in the literature.[1,2,10] Much of the spectacular change in conductivity,[11] optical properties,[12] and superconductivity[13] can be understood in terms of a simple charge transfer model[11] in which electrons are transferred from the guest species to the host lattice. In the case of pyridine intercalation in NbS_2, TaS_2, etc., however, the orientation of pyridine molecules in their van der Waals gap[14,15] disallows any direct interaction between the nitrogen lone pair and the host lattice. The existence of pyridinium ions as an intercalated species has led to the postulation of a different mechanism, the Schöllhorn

(1) Levy, F., Ed. *Intercalated Layered Materials*; D. Riedel: Dordrecht, 1979.
(2) Whittingham, M. S.; Jacobson, A. J., Eds. *Intercalation Chemistry*; Academic: New York, 1982.
(3) Klingen, W.; Ott, R.; Hahn, H. *Z. Anorg. Allg. Chem.* **1973**, *396*, 271-278.
(4) Levy, F., Ed. *Crystallography and Crystal Chemistry of Materials with Layered Structures*; D. Riedel: Dordrecht, 1976.
(5) Wilson, J. A.; Yoffe, A. D. *Adv. Phys.* **1969**, *73*, 193-335.
(6) Brec, R. *Solid State Ionics* **1986**, *22*, 3-30. Johnson, J. W. In ref 2, Chapter 8, pp 267-283.
(7) Joy, P. A. Ph.D. Thesis 1990, IISc, Bangalore.
(8) Piacentini, M.; Grasso, V.; Santangelo, S.; Fanfoni, M.; Modesti, S.; Savoir, A. *Solid State Commun.* **1984**, *51*, 467-471. Ohno, Y.; Hirama, K. *J. Solid State Chem.* **1986**, *63*, 258-266. Grasso, V.; Neri, F.; Santangelo, S.; Silipigni, L.; Piacentini, M. *Phys. Rev.* **1988**, B37, 4419-4424.
(9) Le Flem, G.; Brec, R.; Ouvrard, G.; Louisy, A.; Segransan, P. *J. Phys. Chem. Solids* **1982**, *43*, 455-461.
(10) Whittingham, M. S.; Dines, M. B. *Surv. Prog. Chem.* **1980**, *9*, 55-57. Gamble, F. R.; Geballe, T. H. *Treatise Solid State Chem.* **1980**, *3*, 89-166. *Proc. Int. Conf. Layered Materials and Intercalates, Physica* **1980**, *99B*. Whittingham, M. S. *Prog. Solid State Chem.* **1978**, *12*, 41-99.
(11) Friend, R. H.; Yoffe, A. D. *Adv. Phys.* **1987**, *36*, 1-94.
(12) Beal, A. R.; Liang, W. Y. *Philos. Mag.* **1973**, *27*, 1397-1416. Acrivos, J. V.; Salem, J. R. *Philos. Mag.* **1974**, *30*, 603-619.
(13) Gamble, F. R.; Osiecki, J. H.; Cais, M.; Pisharody, R.; Di Salvo, F.; Geballe, T. H. *Science* **1971**, *174*, 493-497. Subbarao, G. V.; Shafer, M. W.; Tsang, J. C. *J. Phys. Chem.* **1975**, *79*, 553-557.
(14) Riekel, C.; Fischer, C. O. *J. Solid State Chem.* **1979**, *29*, 181-190. Kashihara, Y.; Nishida, A.; Ohshima, K.; Harada, J.; Yoshioka, H. *J. Phys. Soc. Jpn.* **1979**, *46*, 1393-1394.
(15) Tofield, B. C.; Wright, C. J. *Solid State Commun.* **1977**, *22*, 715-718.

0002-7863/92/1514-7792$03.00/0